Applied Catalysis B: Environmental 87 (2009) 200–210

Contents lists available at ScienceDirect

Applied Catalysis B: Environmental

journal homepage: www.elsevier.com/locate/apcatb

Detailed kinetic modeling of NO_x adsorption and NO oxidation over Cu-ZSM-5

Louise Olsson [a,*], Hanna Sjövall [a], Richard J. Blint [b]

[a] Competence Centre for Catalysis, Chemical Reaction Engineering, Chalmers University of Technology, 412 96 Göteborg, Sweden
[b] General Motors R&D Center, Chemical and Environmental Sciences Laboratory, 30500 Mound Road, Warren, MI 48090-9055, United States

ARTICLE INFO

Article history:
Received 27 May 2008
Received in revised form 31 August 2008
Accepted 8 September 2008
Available online 19 September 2008

Keywords:
NO_2
Detailed kinetic modeling
Zeolite
Copper
TPD
Low-temperature activity

ABSTRACT

Detailed kinetic modeling was used in combination with flow reactor experiments to investigate the NO_x adsorption/desorption and NO oxidation over Cu-ZSM-5. NO oxidation is likely an important step for selective catalytic reduction (SCR) using urea and hydrocarbons, and thus was investigated separately. First the NO_2 adsorption on Brönstedt acid sites in H-ZSM-5 was modeled using an NO_2 temperature programmed desorption (TPD) experiment. These results, together with the results of the NO_2 TPD and NO oxidation experiments, were used in developing the model for Cu-ZSM-5. A substantial amount of NO_2 was adsorbed on the catalyst. However, the results from a corresponding NO TPD experiment showed that only very small amounts of NO were adsorbed on the catalyst and therefore this step was not included in the model. The model consists of reversible steps for NO_2 and O_2 adsorption, O_2 dissociation, NO oxidation and two steps for nitrate formation. The first nitrate formation step was disproportionation of NO_2 to form NO and nitrates. This step enabled us to describe the NO production during NO_2 adsorption. Further, in the reverse step the NO reacts with the nitrates and decreased their stability. Without this step the nitrates blocked the surface resulting in to low NO oxidation activity. However, we observe that nitrates can be decomposed also without the presence of NO and in the second reversible step were the nitrates decomposed to form NO_2 and oxygen on the copper. These steps enabled us to describe both the TPD and activity measurement results. NO oxidation was observed even at room temperature. Interestingly, the NO_2 decreased when increasing the temperature up to 100 °C and then increased as the temperature increased further. We suggest that this low-temperature NO oxidation occurs with species loosely bound on the surface and that is included in the detailed mechanism. An additional NO_2 TPD at 30 °C was also modeled to describe the loosely bound NO_2 on the surface. The detailed model correctly describes NO_2 storage, NO oxidation and low-temperature NO oxidation.

1. Introduction

The use of diesel engines and lean-burn gasoline engines decreases the fuel consumption compared to conventional stoichiometric engines. However, a major obstacle is that the three-way catalyst cannot reduce the nitrogen oxides, when there is excess oxygen in the exhaust. It is important to decrease the emissions of NO_x for environmental reasons. There are three major catalytic concepts for reduction of NO_x in lean exhaust gases: NO_x storage and reduction catalysts, urea selective catalytic reduction (urea SCR) and hydrocarbon (HC) SCR.

In urea SCR, the urea (NH_2-CO-NH_2) is injected before the catalyst and is decomposed to ammonia and HNCO, which is hydrolysed as described by the following reactions:

$$NH_2 - CO - NH_2 \rightarrow NH_3 + HNCO \quad (1)$$

$$HNCO + H_2O \rightarrow NH_3 + CO_2 \quad (2)$$

Over the catalyst ammonia reacts selectively with NO and NO_2 to form N_2. There are many catalysts investigated for this system, where vanadia is the most common catalyst [1–7]. Different ion-exchanged zeolites have also been thoroughly investigated, for example Cu-ZSM-5 [8–14], Cu-faujasite [15,16], H-ZSM-5 [17,18], Fe-ZSM-5 [19,20] and Fe-zeolite-beta [21]. There are three major steps for the ammonia SCR:

$$4NH_3 + 4NO + O_2 \rightarrow 4N_2 + 6H_2O \,(\text{standard SCR}) \quad (3)$$

$$2NH_3 + NO + NO_2 \rightarrow 2N_2 + 3H_2O \,(\text{fast SCR}) \quad (4)$$

$$4NH_3 + 3NO_2 \rightarrow 3.5N_2 + 6H_2O \,(\text{slow } NO_2 \text{ SCR}) \quad (5)$$

* Corresponding author. Tel.: +46 31 772 4390; fax: +46 31 772 3035.
E-mail address: louise.olsson@chalmers.se (L. Olsson).

0926-3373/$ – see front matter © 2008 Elsevier B.V. All rights reserved.
doi:10.1016/j.apcatb.2008.09.007

Nomenclature

A_n	monolith wall area in each tank (m^2)
A_j	pre-exponential factor for reaction j, unit depends on rate expression
A_{ads}	pre-exponential factor for adsorption, used for calculating ΔS (s^{-1})
A_{des}	pre-exponential factor for desorption used for calculating ΔS (s^{-1})
c_g	concentration in the gas phase (mol/m^3)
c_s	concentration at the surface of the wash-coat (mol/m^3)
$E_{a,j}$	activation energy for reaction j (J/mol)
$E_{a,j}(0)$	activation energy for reaction j for zero coverage (J/mol)
$F_{i,n}$	molar flow of component i in tank number n (mol/s)
h	Planck's constant (J s)
I_m	rotational moment of inertia in direction m, where $m = x$, y, or z (kg m^2)
k_B	Boltzmann constant (J/K)
k_c	mass-transfer coefficient (m/s)
k_j	rate constant for reaction j, unit depends on rate expression
$m_{wc,n}$	mass of zeolite in tank n (kg)
M	molecule mass (kg)
N_{cat}	number of active sites per mass zeolite (mol/(kg zeolite))
$q_{tr,3D}$	partition function for 3DIM translation
q_{rot}	partition function for rotation
Q	partition function
$r_{j,n}$	rate of reaction j in tank n (mol/(s kg zeolite))
R	gas constant (J/(mol K))
S	entropy (J/(mol K))
S1a	Cu-site
S2	Brönsted acid sites
S3	weak adsorption sites
t	time (s)
T	temperature (K)
V	molecule volume (m^3)

Greek letters

$\alpha_{i,j}$	coverage dependence for specie i in reaction j
ΔS	entropy loss, due to adsorption (J/(mol K))
θ_i	coverage of specie i
$\Theta_{i,n}$	coverage of specie i in tank n
$\nu_{i,j}$	stoichiometric coefficient for component i and reaction j
σ_r	symmetry number

It has been observed over several catalysts that a mix of about 50% NO and 50% NO_2 gives the highest conversion [8,19,22]. In an earlier study we found that the Cu-ZSM-5 could oxidize substantial amounts of NO to NO_2 [8]. Further, we observed large nitrate formation with the use of in situ FTIR [9], when exposing the catalyst to NO and oxygen. Kiovsky et al. [23] suggest that the NO oxidation is the rate limiting step in SCR over zeolite catalysts. However, Eng and Bartholomew [18] concluded that NO oxidation was not rate determining over HZSM-5. These results are in contradiction with the ones from Wallin et al. [24] and Stevenson et al. [17], who both suggest that NO oxidation is the rate limiting step over H-ZSM-5. Devadas et al. [25] suggested that NO oxidation is rate limiting over Fe-ZSM-5.

In HC-SCR the NO_x is reduced by a selective reaction with the hydrocarbons. The catalysts for HC-SCR can be divided into three groups [26], noble metals, zeolites and oxides. In recent years there has been a large interest in Ag/Al_2O_3 [27] and different zeolites for this reaction. There has been a huge amount of different ion-exchanged zeolites investigated for this reaction, examples are; Cu [26], Pt [28], Co [28], Pd [28], Ga [28], In [28], Ce [28], Fe [28] and Rh [28] zeolites. In addition, combinations with different promoters have been studied [28]. Cu-ZSM-5 has been extensively investigated for HC-SCR [26]. There are several different mechanisms described for HC-SCR over Cu-ZSM-5. It is suggested that the first step is the oxidation of NO to NO_2 on the surface over Cu-ZSM-5 [29,30] and H-ZSM-5 [31,32]. In addition, Wang et al. [33] proposed that the HC-SCR using acetylene is controlled by NO oxidation over MoO_3/HZSM-5. The dual pore concept [34] was suggested, since NO oxidation is believed to be important for HC-SCR. In this concept the NO oxidation occurs in zeolites with narrow pores. These pores cannot be accessed by the large hydrocarbons, thus hindering the unwanted HC oxidation. The SCR occurs on another zeolite, with larger pores.

There are only a few global kinetic models presented in the literature for NO oxidation on ion-exchanged zeolites. Brosius et al. [34] presents a global kinetic model for NO oxidation on Fe-ZSM-5 and the same rate expression is also used by Čapek et al. [35] for Cu-ZSM-5. Tomašić et al. [36] modeled NO oxidation over Cu-ZSM-5 using a global rate and Chatterjee et al. [37] present a global model for NO oxidation over a commercial zeolite. Olsson et al. [10] also presents a global rate for NO oxidation when modeling NH_3 SCR over Cu-ZSM-5. However, there are no detailed kinetic models in the literature that describe the NO oxidation and nitrate formation over ion-exchanged zeolites. The objective of this work is therefore to perform experiments and detailed kinetic modeling of NO oxidation and nitrate formation over Cu-ZSM-5. In addition, the low-temperature NO oxidation, occurring at room temperature, is investigated experimentally and a detailed kinetic model is also proposed for this process.

2. Experimental

2.1. Catalyst preparation

The catalysts were prepared using H-ZSM-5 powder, with a SiO_2/Al_2O_3 ratio of 27, from Alsi-Penta. The copper zeolite was prepared in two steps. First the H-ZSM-5 was ion exchanged with $NaNO_3$, to get a controlled ion-exchange followed by ion-exchange with copper ($Cu(CH_3COO)_2$). The cordierite monoliths had a cell density of 400 cpsi and were wash-coated stepwise, using the incipient wetness impregnation method. In order to assist the attachment of the zeolite the cordierite was first impregnated with a thin alumina layer, using 5% boehmite (Disperal D) in a liquid phase containing 50% distilled water and 50% ethanol. This was followed by deposition of the zeolite from a slurry consisting of a solid phase with 80% Cu-ZSM-5 (or HZSM-5) and 20% Boehmite (Disperal D) and a liquid phase composed of 50% distilled water and 50% ethanol. Two Cu-ZSM-5 monoliths were prepared at the same time, using the same slurries. They are denoted Cu-ZSM-5-a and Cu-ZSM-5-b. Details about the ion-exchange and preparation can be found in [8,10]. The length and diameter of the samples were 30 and 22 mm, respectively and information about the samples is given in Table 1.

Table 1
Details about the catalyst samples used.

Sample	SiO_2/Al_2O_3 ratio	Weight alumina layer (mg)	Weight zeolite layer (mg)	Cu loading (wt-%) [8]	Ion-exchange level (Cu/2 Al) [8]
H-ZSM-5 [8]	27	92	1002	–	–
Cu-ZSM-5-a [8]	27	73	1038	2.03	0.70
Cu-ZSM-5-b	27	78	1010	2.03	0.70

2.2. Flow reactor experiments

A flow reactor was used for measuring the activity and storage over the catalysts. The setup is described in [8]. Briefly, it consists of a gas mixing system (Environics 2000) with nine mass flow controllers and a quartz reactor. The temperature of the reactor is controlled using a thermocouple placed a few mm in front of the catalyst. In addition, the temperature was measured in the middle of the catalyst using a second thermocouple. The NO and NO_2 were analysed using a chemiluminescence detector (Eco Physics CLD 700). Ar was the inert balance in all experiments and the total feed flow rate was 3500 ml/min, corresponding to a space velocity of 18,400 h^{-1}. Prior to each experiment, the catalysts were pre-treated with 8% O_2 in Ar at 500 °C for 20 min.

NO_2 TPD experiments were conducted over both the H-ZSM-5 and Cu-ZSM-5-b catalyst. The catalysts were exposed to 500 ppm NO_2 at 150 °C for 80 min, flushed with Ar for 60 min and finally the temperature was linearly increased to 500 °C in Ar with a speed of 10 °C/min. A corresponding NO TPD experiment was performed over the Cu-ZSM-5-b catalyst, where the sample was exposed to 500 ppm NO for 80 min at 150 °C. This was followed by flushing the sample with Ar for 67 min and finally a temperature ramp to 500 °C was conducted, with a speed of 10 °C/min, while exposing the catalyst to Ar only. An additional NO_2 TPD experiments was also conducted on Cu-ZSM-5-b, where the catalyst was exposed to 500 ppm NO_2 and 8% O_2 at about 30 °C for 56 min, followed by Ar for 43 min and finally a temperature ramp to 500 °C was performed when exposing the catalyst to 8% O_2.

Two experiments were conducted in order to investigate the NO oxidation activity over the Cu-ZSM-5-a catalyst. In the first experiment the catalyst was exposed to 500 ppm NO and 8% O_2 and increasing the temperature stepwise from 30 to 500 °C (30, 50, 100, 150, 200, 250, 300, 350, 400, 450 and 500 °C). The time duration was 60 min, for the first step and 20 min for the others. In the second experiment was the sample exposed to 500 ppm NO and 8% O_2 and the temperature was changed stepwise (30 °C for 120 min, 50 °C for 110 min, 100 °C for 60 min, 30 °C for 120 min, 50 °C for 110 min, 100 °C for 40 min).

3. The model

3.1. Mathematical model

In this model, the monolith is described as a series of continuously stirred tank reactors. In order to estimate the number of elements needed we used a combination of the dispersion model and tanks-in-series model [38], which resulted in about 40 tanks. However, the computational time would be long using 40 tanks and Westerberg et al. [39] used 10 instead of 40–140 in their simulations of HC-SCR. We also chose to use 10 elements in this study. The error when comparing 10 and 15 tanks was less than 0.3% (the error were calculated using 12 experiments, including ammonia and water adsorption, NH_3 oxidation, NO oxidation and several NH_3 SCR experiments). Further, the model assumes no accumulation in the gas phase, no diffusion limitations in the wash-coat and no radial concentration gradients. In an earlier publication [10] we experimentally examined the mass-transfer in the wash-coat for Cu-ZSM-5 using two catalysts, the first with 23 weight% wash-coat and the second with 11%. The flow rate was decreased to 50% for the sample with the thinner wash-coat. Thus there was a constant ratio between zeolite mass and flow rate. We observed the same NH_3 SCR conversion for both catalysts. These results indicate that there are no mass-transfer limitations in the wash-coat [10]. The film model is used to describe the mass-transfer from the gas to the surface. The mass balance for each gas component (i) in each tank (n) is:

$$F_{i,n-1} - F_{i,n} - k_{c,i,n} A_n (c_{g,i,n} - c_{s,i,n}) = 0 \quad (6)$$

The surface balances are:

$$k_{c,i,n} A_n (c_{g,i,n} - c_{s,i,n}) = \sum_j \nu_{i,j} r_{j,n} m_{wc,n} \quad (7)$$

$$N_{cat} \frac{\partial \Theta_{i,n}}{\partial t} = \sum_j \nu_{i,j} r_{j,n} \quad (8)$$

3.2. Surface description

The ion-exchange level of Cu was determined to 0.70 (Cu/2 Al), using ICP-AES (Inductively Coupled Plasma and Atomic Emission Spectrometry) [8]. This was used to calculate the number of copper sites in the catalyst (S1a). On this site is NO_2 and O_2 adsorbed and the reaction occurs on this site. The surface description is more thoroughly described in a paper where NH_3 adsorption is investigated [11]. Briefly, Komatsu et al. [40] propose that each copper ion can coordinate four ammonia molecules. This is also experimentally observed using Electron paramagnetic resonance studies (EPR) [41,42] and by density functional theory calculations [43]. In our model we therefore use that four ammonia can coordinate to each copper and introduce S1b which is three times the number of S1a, to add up to four ammonia per copper (S1a + 3S1b per copper). Since NO_2 TPD experiments in this work have shown that much less NO_x is stored compared to ammonia on Cu-ZSM-5 the NO_2 is only adsorbed on S1a in the model. Further, the Si/Al ratio was 27 and this was used to calculate the number of Brönstedt acid sites (S2), by using 70% ion-exchange (Cu/2Al) and that each copper coordinates to two Al. Further, both ammonia [11] and NO_2 adsorbs large quantities at low temperatures and it was therefore necessary to introduce S3, for loosely bound species. Loosely bound NO_x species (physisorbed) was also proposed by Grossale et al. [44] over Fe zeolites. The number of S3 sites were determined by storage of ammonia at room temperature [11], compensating for storage on copper and Brönstedt acid sites. The resulting number of sites for S1a, S2 and S3 for the three catalysts used is shown in Table 2. Since the same zeolite powder was used for Cu-ZSM-5-a and Cu-ZSM-5-b they have the same number of sites per wash-coat weight. These catalysts are prepared at the same time, using the same slurries and they contain very similar amounts of zeolite (1038 and 1010 mg). In addition, after the initial stabilisation the samples gave the same conversion (only about 5 ppm difference).

Table 2
Number of sites in the model [11].

Sample	Cu-sites, S1a (mol/kg zeolite)	Brönsted acid sites, S2 (mol/kg zeolite)	Weak adsorption sites, S3 (mol/kg zeolite)
H-ZSM-5	–	0.928	1.227
Cu-ZSM-5-a	0.320	0.288	1.227
Cu-ZSM-5-b	0.320	0.288	1.227

3.3. Determination of rate parameters

The rate constants are described with the Arrhenius expression:

$$k_j = A_j e^{-E_{a,j}/RT} \tag{9}$$

In the parameter fitting was a centred Arrhenius expression used in order to decrease the correlation between the pre-exponential factors and activation energies, using 600 K as the reference temperature. All the pre-exponential factors given in the result section are on the standard form, shown in Eq. (9). In the NO_2 TPD the desorption peak for NO_2 was broad, suggesting that NO_2 are adsorbed on the surface with different energies. Therefore, coverage-dependent activation energies were used for some of the desorption steps:

$$E_{a,j} = E_{a,j}(0)(1 - \alpha_{i,j} \cdot \theta_i) \tag{10}$$

The pre-exponential factors for most of the desorption steps and reaction steps are fixed to $10^{13}\ s^{-1}$, see Tables 6–8. Since the channels in the zeolite are very narrow, we chose not to calculate the pre-exponential factors for adsorption with the kinetic gas theory. Instead, we calculated them using an estimate of the entropy change according to

$$\Delta S = R \cdot \ln\left(\frac{A_{ads}}{A_{des}}\right) \tag{11}$$

The entropy was calculated with the use of the partition functions, q

$$S = R \cdot \ln(q) + RT\frac{d(\ln(q))}{dT} \tag{12}$$

The partition function (q) for rotation and translation can be calculated according to

$$q_{tr,3D} = \frac{(2\pi m k_B T)^{3/2}}{h^3} V \tag{13}$$

$$q_{rot} = \frac{8\pi^2\sqrt{8\pi^3 I_x I_y I_z}(k_B T)^{3/2}}{\sigma_r h^3} \quad \text{non-linear molecule} \tag{14}$$

$$q_{rot} = \frac{(8\pi^2 I_x k_B T)}{\sigma_r h^2} \quad \text{linear molecule} \tag{15}$$

According to Sharma et al. [45] ammonia adsorbed on H-ZSM-5 looses the translational entropy and approximately one third of the local entropy (rotation and vibration). We assume that the compounds will adsorb as localised species and they therefore lose all translational entropy and in addition one third of the rotational entropy. The loss in vibrational entropy is omitted, due to that it is much smaller compared to the translational and rotational entropy. The calculated entropy changes are −174.3, −215.6 and −188.3 J/(mol K) for O_2, NO and NO_2, respectively. The reference temperature used was 600 K.

Some of the parameters were determined from thermodynamic restrictions. The parameters that were not fixed were fitted to the experiments using the least square method.

3.4. The kinetic model

3.4.1. Kinetic model for NO_x adsorption over H-ZSM-5

One NO_2 TPD experiment, with the adsorption part at 150 °C, was used for developing the model. We observed that a significant amount of NO_2 adsorbed on the H-ZSM-5 catalyst and therefore included a reaction step for adsorption and desorption of NO_2 on S2 in the model. In addition, was a small NO peak visible during adsorption, which is likely due to disproportionation of NO_2 to form nitrates and NO. This has been observed and suggested for several catalysts; BaO/Al_2O_3 [46], Al_2O_3 [47], BaNa-Y [48], BaO/TiO_2 [49] and over Cu-ZSM-5 [50] and Fe zeolite [44]. However, for HZSM-5 we observe only one NO produced for about six (5.7) NO_2 consumed. This is due to that there is a total uptake of NO_2 for about 2 min without any NO production and the NO is first observed after 3 min. We therefore suggest that the most important step for NO_2 storage over HZSM-5 is a direct NO_2 adsorption step. Further, since the primary objective of this work is to describe the NO_x adsorption and NO oxidation on Cu-ZSM-5, we chose to us as simple model as possible for H-ZSM-5 and did therefore not introduce the disproportionation step. In addition, when assuming the same amount of NO produced on the acid sites in Cu-ZSM-5 and using the amount of sites shown in Table 2, it results in that only about 10% of the NO formed in the NO_2 TPD over Cu-ZSM-5 is from the acid sites. The reaction and rate expressions are given in Eq. (16) below.

$$NO_2 + S2 \underset{r_{1,b}}{\overset{r_{1,f}}{\leftrightarrow}} NO_2 - S2 \quad r_{1,f} = k_{1,f} c_{NO_2} \theta_{S2-vacant}; \quad r_{1,b} = k_{1,b} \theta_{NO_2-S2} \tag{16}$$

As described above, one NO_2 TPD experiment with the adsorption part at 150 °C, was used. Since the temperature in the experiment is quite high, there was no adsorption of NO_2 on the weakly adsorbed sites included.

3.4.2. NO_2 adsorption and NO oxidation over Cu-ZSM-5

The model for NO_2 adsorption and NO oxidation over Cu-ZSM-5 were developed using three experiments: (i) NO_2 TPD at 150 °C using 500 ppm NO_2 (ii) NO_2 TPD at 30 °C using 500 ppm NO_2 and 8% O_2 and (iii) NO oxidation from room temperature to 500 °C using 500 ppm NO and 8% O_2. The model contains reaction steps for adsorption and desorption of NO_2 and oxygen on copper sites (S1a). The oxygen is assumed to adsorb first molecularly and then dissociate to oxygen atoms on the surface. NO TPD experiments showed that only very small amounts of NO were adsorbed on the surface and therefore the NO adsorption was ignored. This is further discussed in Section 4. The NO oxidation was described by an Eley-Rideal mechanism where the NO from the gas phase reacts directly with oxygen atoms on the copper. The reactions and rate expressions are shown in Table 3.

In a previous FTIR study [9] we observed large formation of nitrites/nitrates on the surface, which also have been seen by others [51–53]. In addition, when exposing the Cu-ZSM-5 catalyst

Table 3
Reactions and rate expressions for NO_2 adsorption and desorption and NO oxidation on copper (S1a) in Cu-ZSM-5.

Reaction	Reaction rate
$NO_2 + S1a \underset{r_{2,b}}{\overset{r_{2,f}}{\leftrightarrow}} NO_2 - S1a$	$r_{2,f} = k_{2,f} c_{NO_2} \theta_{S1a-vacant}; \quad r_{2,b} = k_{2,b} \theta_{NO_2-S1a}$
$O_2 + S1a \underset{r_{3,b}}{\overset{r_{3,f}}{\leftrightarrow}} O_2 - S1a$	$r_{3,f} = k_{3,f} c_{O_2} \theta_{S1a-vacant}; \quad r_{3,b} = k_{3,b} \theta_{O_2-S1a}$
$O_2 - S1a + S1a \underset{r_{4,b}}{\overset{r_{4,f}}{\leftrightarrow}} 2O - S1a$	$r_{4,f} = k_{4,f} \theta_{O_2-S1a} \theta_{S1a-vacant}; \quad r_{4,b} = k_{4,b} \theta^2_{O-S1a}$
$NO + O - S1a \underset{r_{5,b}}{\overset{r_{5,f}}{\leftrightarrow}} NO_2 - S1a$	$r_{5,f} = k_{5,f} c_{NO} \theta_{O-S1a}; \quad r_{5,b} = k_{5,b} \theta_{NO_2-S1a}$

Table 4
Reactions and rate expressions for nitrate formation on Cu-ZSM-5.

Reaction	Reaction rate
$2NO_2 - S1a \underset{r_{6,b}}{\overset{r_{6,f}}{\leftrightarrow}} NO_3 - S1a + NO + S1a$	$r_{6,f} = k_{6,f}\theta^2_{NO_2-S1a}$; $r_{6,b} = k_{6,b}\theta_{NO_3-S1a}c_{NO}\theta_{S1a-vacant}$
$NO_2 - S1a + O - S1a \underset{r_{7,b}}{\overset{r_{7,f}}{\leftrightarrow}} NO_3 - S1a + S1a$	$r_{7,f} = k_{7,f}\theta_{NO_2-S1a}\theta_{O-S1a}$; $r_{7,b} = k_{7,b}\theta_{NO_3-S1a}\theta_{S1a-vacant}$

to NO_2 is an NO peak visible. This is likely due to disproportionation of NO_2 to form NO and nitrates, which has been observed previously for both Cu-ZSM-5 [50] and Fe zeolite [44]. This is also seen for many other materials, like BaO/Al_2O_3 [46], Al_2O_3 [47], BaNa-Y [48] and BaO/TiO_2 [49]. Further, Despres et al. [50] observed that the nitrates were less stable when adding NO to the gas phase. Based on these findings we added one reaction step for the NO_2 disproportionation route (reaction (6), Table 4). However, this step for nitrate formation and decomposition is not sufficient since the nitrates can be decomposed also without the presence of NO, which reaction (6) requires. We therefore added one additional reversible reaction step where nitrates can be decomposed directly to form NO_2 and O on the copper sites (reaction (7), Table 4). This step is similar to the one Apostolescu et al. [47] suggested, where the nitrates decomposes directly to NO_2 and oxygen in the gas phase. The summation of reaction step 6 and 7 results in the following global step

$$3NO_2 - S1a + O - S1a \leftrightarrow 2NO_3 - S1a + NO(g) + 2S1a \quad (17)$$

The overall reaction leads to the production of 1 mol NO for every 3 mol NO_2 adsorbed. Indeed the experimental results in Fig. 1 gives a ratio of NO_2 adsorption per NO produced of 3.0. This is in line with the mechanism proposed by Grossale et al. [44] for a Fe zeolite:

$$3NO_2 + O^{2-} \leftrightarrow 2NO_3{}^- + NO \quad (18)$$

We observed an activity for low-temperature NO oxidation. There was a substantial amount of NO_2 formed at room temperature, however at 50 °C the NO_2 concentration drops and starts to increase again at about 150 °C again. Halasz et al. [32] also observed this over H-ZSM-5. Since this occurs also on a catalyst without copper, this step does not require the copper sites. We suggest that this NO oxidation occurs with species physisorbed on the catalyst. In the model we therefore introduce adsorption and desorption of NO_2 and oxygen on S3 sites together with a step for NO oxidation. The mechanism is shown in Table 5.

4. Results and discussion

One NO_2 TPD experiment was conducted over the Cu-ZSM-5-b catalyst. The sample was exposed to 500 ppm NO_2 at 150 °C for 80 min and flushed with Ar for 60 min at the same temperature before a temperature ramp was performed. The results are shown in Fig. 1. The amount of stored NO_x is the difference between the inlet NO_2 curve and the outlet NO_x curve. The catalyst stores a substantial amount of NO_2. In the initial part of the adsorption period NO is

Table 5
Reactions and rate expressions for low-temperature NO oxidation on Cu-ZSM-5.

Reaction	Reaction rate
$O_2 + 2S3 \underset{r_{I,b}}{\overset{r_{I,f}}{\leftrightarrow}} 2O - S3$	$r_{I,f} = k_{I,f}c_{O_2}\theta^2_{S3-vacant}$; $r_{I,b} = k_{I,b}\theta^2_{O-S3}$
$NO + O - S3 \underset{r_{II,b}}{\overset{r_{II,f}}{\leftrightarrow}} NO_2 - S3$	$r_{II,f} = k_{II,f}c_{NO}\theta_{O-S3}$; $r_{II,b} = k_{II,b}\theta_{NO_2-S3}$
$NO_2 + S3 \underset{r_{III,b}}{\overset{r_{III,f}}{\leftrightarrow}} NO_2 - S3$	$r_{III,f} = k_{III,f}c_{NO_2}\theta_{S3-vacant}$; $r_{III,b} = k_{III,b}\theta_{NO_2-S3}$

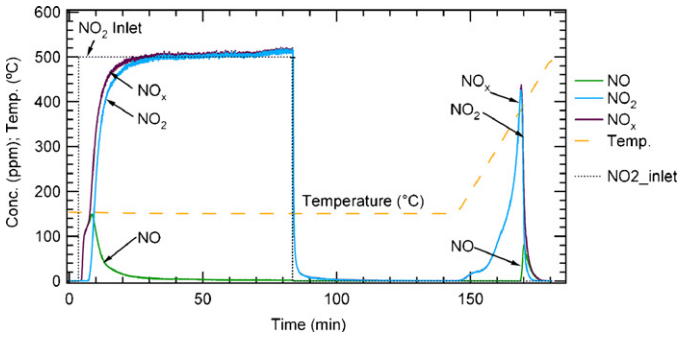

Fig. 1. Measured concentrations of NO, NO_2 and NO_x from an NO_2 TPD experiment conducted at 150 °C over Cu-ZSM-5-b. The catalyst is exposed to 500 ppm NO_2 at 150 °C for 80 min, flushed with Ar for 60 min and finally the temperature is linearly increased to 500 °C in Ar.

released. This is probably due to a disproportion reaction from NO_2 to produce NO and nitrates. This has been observed for several catalysts, and is described in more detail in Sections 3.4.1 and 3.4.2. The nitrate formation is also confirmed by in situ FTIR measurements on Cu-ZSM-5 [9]. When flushing the catalyst with Ar small amounts of NO_2 are desorbed. In the temperature ramp a large release of NO_x is observed. NO_x consists mainly of NO_2, but also a small peak of NO is observed at high temperatures. This is likely due to NO_2 dissociation on the copper sites.

A similar experiment was conducted, where NO was adsorbed instead. In Fig. 2a a comparison is shown between the desorbed NO_x during the NO and the NO_2 TPD, respectively. The catalyst stores substantially more NO_2 compared to NO. The NO_x from the

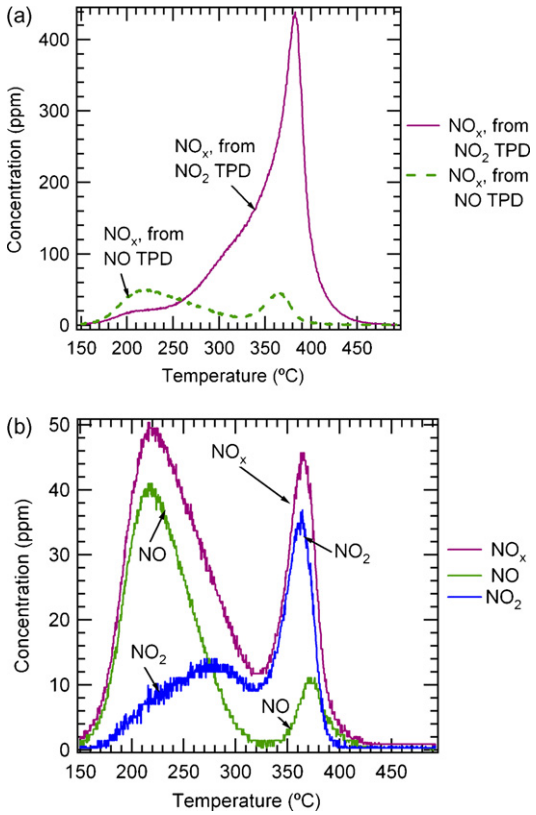

Fig. 2. The Cu-ZSM-5-b catalyst was exposed to 500 ppm NO at 150 °C, which was followed by exposing the sample to Ar and conducting a temperature ramp. (a) The NO_x concentration during the temperature ramp is shown together with the results from a corresponding NO_2 TPD. (b) Measured concentrations of NO, NO_2 and NO_x from the NO TPD experiment.

NO TPD is also released at a lower temperature, due to that these species are more loosely bound compared to the nitrates. The corresponding NO and NO_2 concentrations from the NO TPD experiment are shown in Fig. 2b. The first desorption peak consists of mainly NO. However, the high temperature peak consists of mainly NO_2. This peak also coincides in temperature with the nitrate peak from the NO_2 TPD, see Fig. 2a. We therefore suggest that there is some oxygen on the copper sites when starting the NO exposure, which results in a small amount of formed nitrates. It is possible that small amounts of oxygen are remained on the surface from the pre-treatment at 500 °C with 8% O_2.

4.1. Kinetic model for NO_x adsorption over H-ZSM-5

The H-ZSM-5 catalyst also stores NO_2. In Fig. 3a, the results of a NO_2 TPD experiment, with the adsorption part conducted at 150 °C is shown. There are three desorption peaks from this sample. The main peak occurs at 330 °C (130 ppm at 166 min), and two smaller peaks are observed at about 210 °C (40 ppm at 154 min) and at 420 °C (70 ppm at 175 min). The HZSM-5 catalyst stores less NO_x compared to the Cu-ZSM-5-b catalyst. The maximum desorption peak is about 130 ppm for HZSM-5 and 440 ppm for Cu-ZSM-5-b. Further, the temperature for the main peak is lower for the H-ZSM-5 sample, 330 °C compared to 380 °C. This shows that the nitrates are more stable on the copper sites than on most of the acid sites.

A model was developed to describe this NO_2 storage. Since the primary objective of this work is to describe the NO_x adsorption and NO oxidation on Cu-ZSM-5, we chose to have a very simple model for the H-ZSM-5, containing only one reversible adsorption and desorption step, see Eq. (1). There is an NO peak visible during adsorption likely due to disproportionation of NO_2 to form nitrates and NO. However, as discussed above, only one NO is produced per six NO_2 consumed, which show that the most important adsorption route over H-ZSM-5 is NO_2 adsorption. It should be noted that there is a complete uptake of NO_2 for about two min without any NO production. In addition, there are less acid sites available in the Cu-ZSM-5 sample and it is estimated that only about 10% of the NO produced on the Cu-ZSM-5 catalyst origins from the acid sites (Section 3.4.1). We do not attempt to describe this nitrate formation on the Brönstedt acid sites, since (i) it will not be crucial for the development of the overall model and (ii) only one NO is produced per 6 NO_2 stored, showing that NO_2 adsorption is the primary route on this catalyst.

Table 6
Kinetic parameters for NO_x adsorption over H-ZSM-5.

Rate	Rate constants	Pre-exponential factor	Activation energy (kJ/mol)	Coverage dependence (α)
NO_2 adsorption	$k_{1,f}$	4.90×10^{1}[a,b]	0	–
NO_2 desorption	$k_{1,b}$	6.76×10^{12}[c,d]	171.60 ± 0.27	$-1.0 \times (\theta_{NO_2-S2})$

[a] $m^3/(s\ kg\ zeolite)$.
[b] Calculated from entropy loss.
[c] mol/(s kg zeolite).
[d] Fixed to $10^{13}\ s^{-1}$.

The resulting NO and NO_x concentrations predicted from the model are also shown in Fig. 3a. The calculated mean coverage on the surface is shown in Fig. 3b. The model can describe the amount of stored NO_x well. The NO_x released in the temperature ramp consists of three peaks experimentally. Thus, NO_2 is adsorbed on different types of sites in this catalyst. However, since we want to use a model as simple as possible, we chose to describe this with a broad NO_x peak, using a coverage-dependent activation energy. The kinetic parameters and their linearized 95% confidence intervals are shown in Table 6. The limits for the parameter $\alpha_{1,b}$ that describes the coverage dependence were between 0 and 1. We observed the minimum squares of errors using the limit $\alpha_{1,b} = 1$, and this parameter was therefore fixed to this value.

4.2. Kinetic model for NO_x adsorption and NO oxidation over Cu-ZSM-5

A model for NO_2 adsorption/desorption and NO oxidation on Cu-ZSM-5 was developed. The NO_2 TPD experiment shown in Fig. 1 was used in the modeling of NO_2 adsorption and desorption. The

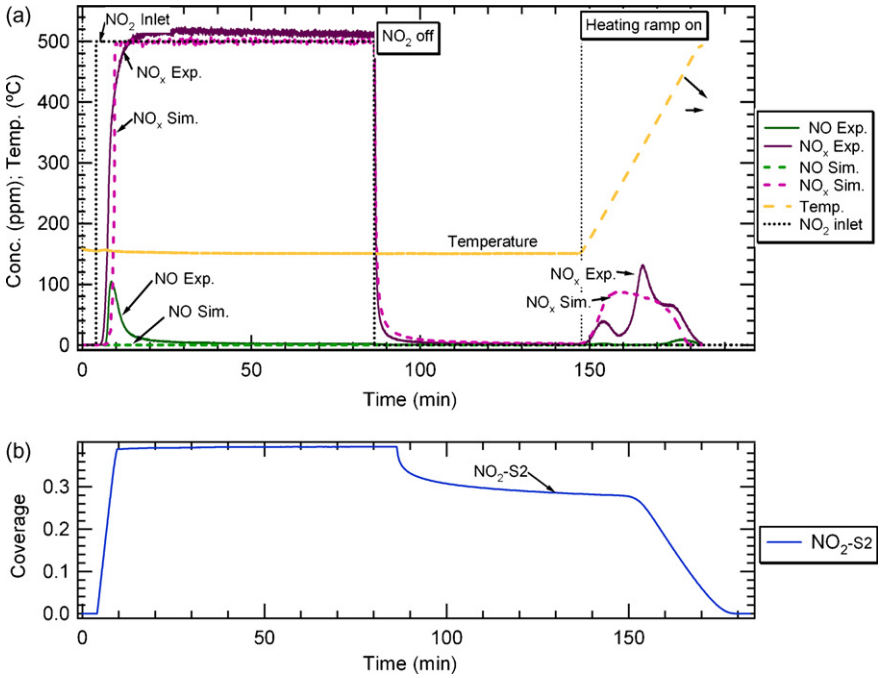

Fig. 3. (a) Measured and calculated concentrations during NO_2 TPD experiment conducted at 150 °C over H-ZSM-5. The mechanism is described in Eq. (1). (b) Calculated mean coverage on the surface.

NO adsorption was very small compared to the NO_2 adsorption, which was shown in Fig. 2b. The NO adsorption was therefore not included in the model. The mechanism contains seven reversible reaction steps, with the first five being: NO_2 adsorption/desorption on Brönstedt sites, NO_2 and O_2 adsorption/desorption on copper sites, oxygen dissociation/recombination and NO oxidation/NO_2 dissociation. The formation and decomposition of nitrates were described by two reversible reactions. In the first reaction nitrates are formed from the NO_2 disproportionation with a simultaneous release of NO. The reversible reaction describes that the nitrates are less stable in the presence of NO, which is in accordance with a study by Despres et al. [50]. The nitrates are decomposed without the presence of NO, but with a lower rate, and this is described in the second reversible reaction where nitrates are decomposed to form NO_2 and O on the copper sites. The sum of these two steps add up to ratio of one NO produced per three NO_2 consumed during storage, which was also observed experimentally. This is in line with the mechanism proposed by Grossale et al. [44] over Fe zeolites. The adsorption of NO_2 on the Brönstedt acid sites was included, as described above, and the parameters given in Table 6 were used. The pre-exponential factors for adsorption and desorption of NO_2 on S2 was recalculated for the change in number of Brönstedt acid sites on the Cu-ZSM-5 samples. All reaction steps are shown in Eq. (1) and Tables 3 and 4. The measured and simulated NO and NO_x concentration from the NO_2 TPD at 150 °C are shown in Fig. 4a. The corresponding calculated mean coverages on the surface are shown in the lower panel of the figure. The model can describe the amount of stored NO_2 and the initial NO formation well. In the model the NO release is due to nitrate formation. Further, the model can adequately describe the release of NO_2 and NO during the temperature ramp. The calculated coverages show that the model predicts an initial formation of NO_2 on the copper sites. These are slowly transformed to nitrates and there is desorption of NO in the gas phase occurring simultaneously, which coincides with NO measured experimentally. At higher temperatures the nitrates are decomposed. The model also predicts adsorption of NO_2 on the Brönstedt acid sites.

The measured and simulated concentrations for the NO oxidation experiment over the Cu-ZSM-5-a catalyst are shown in Fig. 5a. The corresponding calculated mean coverages on the surface are shown in Fig. 5b. In this experiment the catalyst is exposed to 500 ppm NO and 8% O_2 and the temperature is increased stepwise from 25 to 500 °C. At room temperature there is substantial formation of NO_2, which is decreased when the temperature is increased. This was also observed by Halasz et al. [32] over H-ZSM-5. The NO_2 concentration starts to increase at 150 °C again and reaches a maximum at 350 °C. Desorption of NO_x is observed when increasing the temperature. The model can describe the NO oxidation between 250 and 500 °C well. The reason for the increase in NO_2 concentration when increasing the temperature between 150 and 350 °C is that this reaction is kinetically limited. At higher temperatures the NO and NO_2 concentrations follow the thermodynamic levels, which is the reason for the decrease in NO_2 at higher temperatures. The model is further developed to describe the low-temperature NO oxidation and this is described thoroughly below. The calculated coverages on the surface (Fig. 5b) show that NO_2 on copper sites and Brönstedt acid sites build up slowly at lower temperatures. If the model had described the NO_2 formation at room temperature adequately, the catalyst would be saturated with NO_x at a low temperature and the simulated NO_2 in the outlet of the catalyst would have occurred at a lower temperature than is observed in Fig. 5a. Further, at 200 °C the NO_2 on copper is converted to nitrates in the model and the coverage of the nitrates starts to decrease at 350 °C. In the model the coverages of nitrates are much lower for the NO oxidation experiment compared to the NO_2 TPD experiment. For example at 250 °C the coverage of nitrates is about 0.9 in the TPD, however for the NO oxidation simulation it is only about 0.35. The reason is reaction step 6, where the nitrates react with NO in the gas phase. This reaction step is supported by experiments performed by Despres et al. [50]. They found that NO could increase the release of already stored NO_x on a Cu-ZSM-5. They suggest that the reason is that NO interacts with the nitrates, resulting in lower stability of the nitrates. We found that this

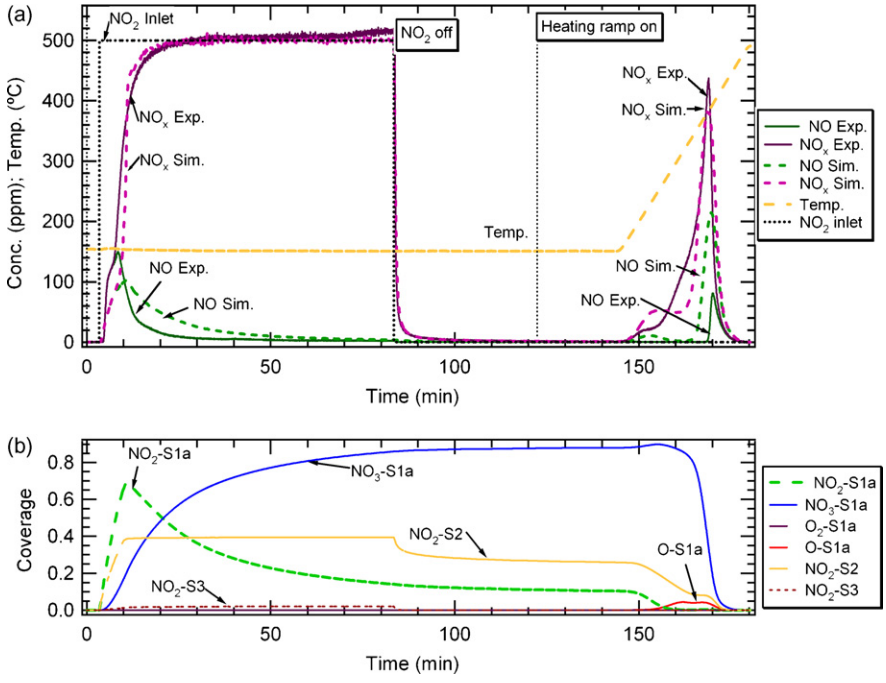

Fig. 4. (a) Measured and calculated concentrations during NO_2 TPD experiment conducted at 150 °C over Cu-ZSM-5-b. The mechanism is described in Eq. (1) and Tables 3 and 4. No steps are added for low-temperature activity. (b) Calculated mean coverage on the surface.

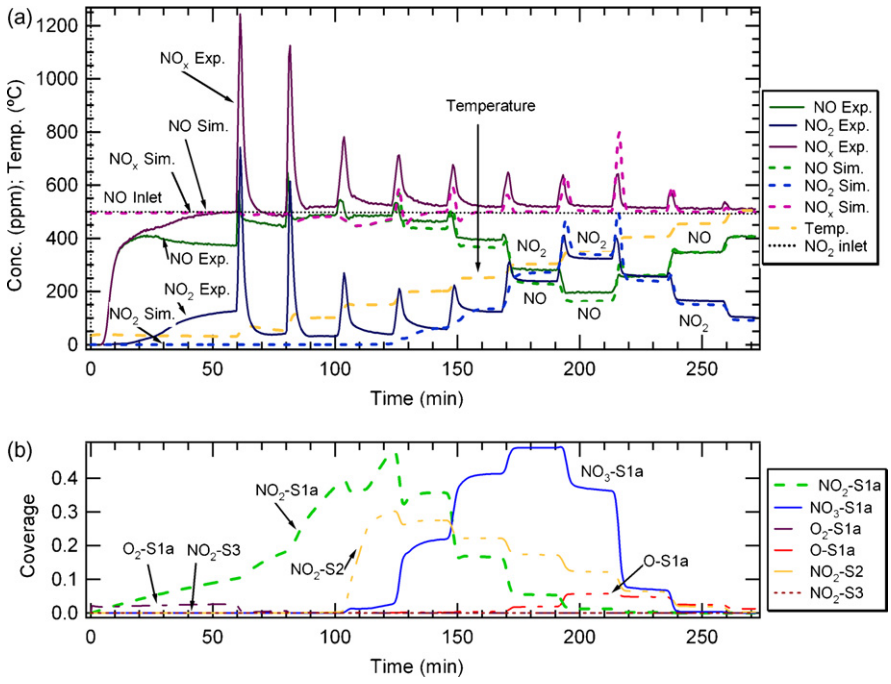

Fig. 5. (a) Measured and calculated concentrations during the NO oxidation experiment over Cu-ZSM-5-a. The mechanism is described in Eq. (1) and Tables 3 and 4. No steps are added for low-temperature activity. (b) Calculated mean coverage on the surface.

reaction step was crucial for describing the NO_2 TPD and NO oxidation experiment simultaneously. Without this step the copper would have been covered with nitrates during the NO oxidation experiment, resulting in prediction of very low NO_2 concentrations.

The low-temperature NO oxidation over Cu-ZSM-5-a was investigated further. First was the NO oxidation in an empty reactor measured, to ensure that there was no gas phase activity. The empty reactor experiments were conducted both at 25 °C and stepwise between 150 and 650 °C. There is a constant very low NO_2 concentration detected (10–15 ppm). This is likely due to small NO_2 residues in the gas bottle or in the calibration of the detector, since the level is so low and does not change with temperature. The results clearly show that there are no NO oxidation occurring in the gas phase. In order to examine the low-temperature oxidation on Cu-ZSM-5 in more detail the catalyst was exposed to 500 ppm NO and 8% O_2 and the temperature was changed stepwise (30 °C for 120 min, 50 °C for 110 min, 100 °C for 60 min, 30 °C for 120 min, 50 °C for 110 min, 100 °C for 40 min). The resulting NO, NO_2 and NO_x concentrations are shown in the lower panel of Fig. 6 and in the upper panel the temperature is shown. At room temperature about 160 ppm NO_2 is formed, but increasing the temperature by 20 °C results in a decrease to 60 ppm NO_2. This is even further decreased to about 30 ppm at 100 °C. The temperature is again decreased to room temperature and after that increased to 50 and 100 °C. The results show that the low-temperature NO oxidation is reproduced regardless of the direction of the temperature change.

In the model, the low-temperature NO oxidation was described by species physisorbed on the catalyst. Oxygen adsorbs loosely on S3 and NO_2 on S3 is formed by an Eley-Rideal mechanism with NO in the gas phase. One step for adsorption and desorption of NO_2 is also added. In order to fit the parameters for the NO_2 adsorption and desorption one additional NO_2 TPD was conducted at about 30 °C. The catalyst stores about 3.5 times more NO_x at 30 °C compared to at 150 °C, which shows the importance of NO_2 storage on S3 at low temperatures. The results from the simulations and

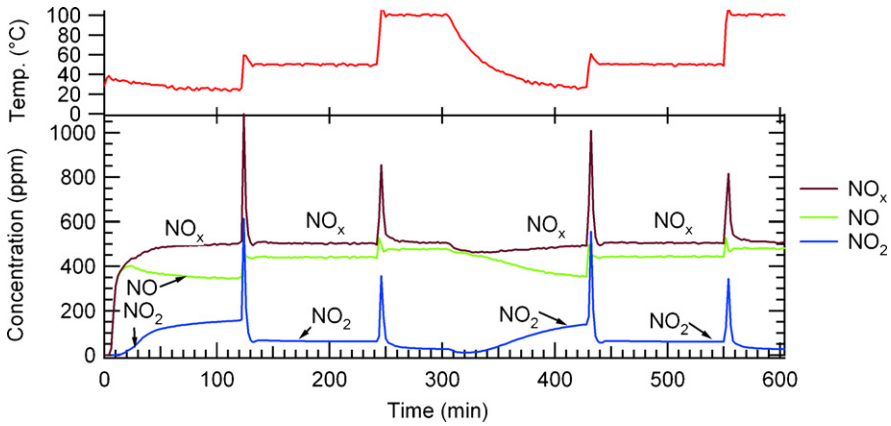

Fig. 6. Measured NO, NO_2 and NO_x concentrations when exposing the Cu-ZSM-5-a catalyst to 500 ppm NO and 8% O_2 and stepwise changing the temperature (30 °C for 120 min, 50 °C for 110 min, 100 °C for 60 min, 30 °C for 120 min, 50 °C for 110 min, 100 °C for 40 min). The temperature is shown in the upper panel.

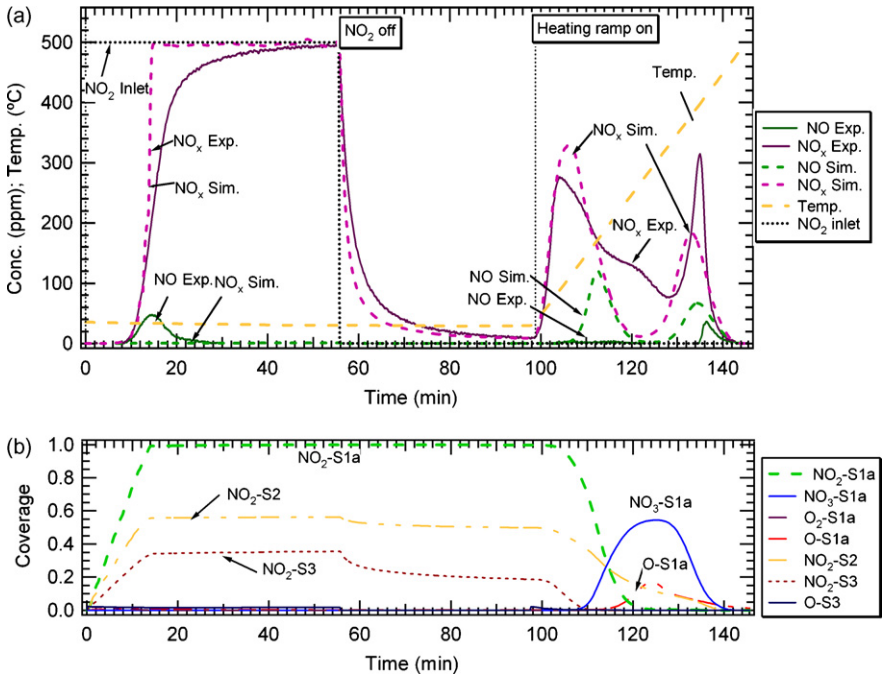

Fig. 7. (a) Measured and calculated concentrations during NO_2 TPD experiment conducted at 30 °C over Cu-ZSM-5-b. The mechanism is described in Eq. (1) and Tables 3–5. Steps are added for low-temperature activity. (b) Calculated mean coverage on the surface.

the experiment are shown in Fig. 7. First there is a total uptake of NO_2 for about 10 min, which the model describes accurately. After storage the catalyst is flushed with Ar and the loosely bound NO_2 from S3 is released, which also corresponds well to the NO_2 out from the catalyst. In the temperature ramp there is experimentally three peaks observed at about 90, 240 and 400 °C (105, 120 and 135 min). Three desorption peaks are also reported for Fe-ZSM-5 by Grossale et al. [44]. The first peak is described by the model by a combination of NO_2 released from S3, S2 and S1a. The second peak at 240 °C observed experimentally is not described by the model. However, there is a release of NO_2 from both S1a and S2 at this temperature, but the released NO_2 is in the model re-adsorbed to form nitrates. The third desorption peak occurring at 400 °C (135 min) is described by the model as decomposition of the stable nitrates on the copper sites. When comparing the results with the TPD conducted at 150 °C (Fig. 4) it is observed that the NO_2 release at 240 °C is much smaller for the 150 °C TPD (20 ppm NO_2 versus 130 ppm). However, the high temperature peak is larger for the

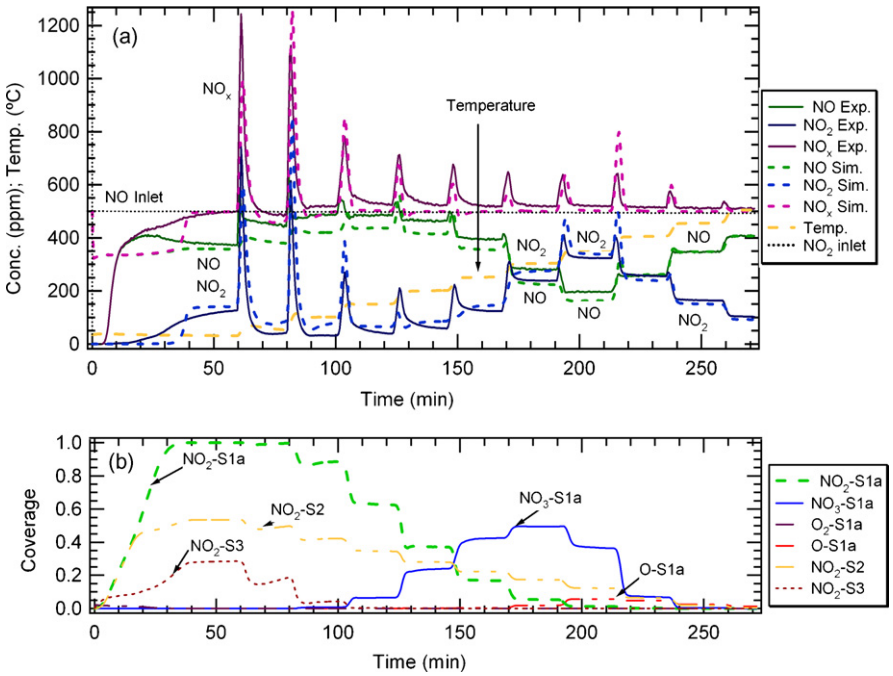

Fig. 8. (a) Measured and calculated concentrations during the NO oxidation experiment over Cu-ZSM-5-a. The mechanism is described in Eq. (1) and Tables 3–5. Steps are added for low-temperature activity. (b) Calculated mean coverage on the surface.

Table 7
Kinetic parameters for NO_x adsorption over Cu-ZSM-5.

Rate	Rate constants	Pre-exponential factor	Activation energy (kJ/mol)	Coverage dependence (α)
NO_2 adsorption	$k_{2,f}$	2.32×10^{1}[a,b]	0.0	
NO_2 desorption	$k_{2,b}$	3.20×10^{12}[c,d]	141.5 ± 0.56	$0.276 \pm 0.0077 \times (\theta_{NO_2-S1a})$
O_2 adsorption	$k_{3,f}$	1.23×10^{2}[a,b]	0.0	
O_2 desorption	$k_{3,b}$	3.20×10^{12}[c,d]	48.8 ± 2.59	
O_2 dissociation	$k_{4,f}$	$3.21 \times 10^{10} \pm 1.8 \times 10^{10}$[c]	83.3 ± 1.9	
O_2 recombination	$k_{4,b}$	3.20×10^{12}[c,d]	161.4 ± 1.83	$0.484 \times (\theta_{NO_2-S1a})$[e]
NO oxidation	$k_{5,f}$	1.16×10^{2}[a,b]	8.9 ± 1.11	
NO_2 dissociation	$k_{5,b}$	3.99×10^{11}[c,e]	145.2[e]	
Nitrate formation	$k_{6,f}$	2.55×10^{12}[c,e]	128.0[e]	
Nitrate decomposition	$k_{6,b}$	1.16×10^{2}[a,b]	19.5[e]	$1.00 \pm 0.061 \times (\theta_{NO_3-S1a})$
Nitrate formation	$k_{7,f}$	3.20×10^{12}[c,d]	167.4 ± 0.22	
Nitrate decomposition	$k_{7,b}$	$5.01 \times 10^{11} \pm 0.57 \times 10^{11}$[c]	195.3 ± 3.4	$0.100 \pm 0.0059 \times (\theta_{NO_3-S1a})$

[a] $m^3/(s\ kg\ zeolite)$.
[b] Calculated from entropy loss.
[c] mol/(s kg zeolite).
[d] Fixed to $10^{13}\ s^{-1}$.
[e] Thermodynamic restriction.

Table 8
Kinetic parameters for NO_x adsorption, desorption and NO oxidation over S3.

Rate	Rate constants	Pre-exponential factor	Activation energy (kJ/mol)	Coverage dependence (α)
NO_2 adsorption	$k_{I,f}$	9.79×10^{1}[a,b]	0.0	
NO_2 desorption	$k_{I,b}$	1.35×10^{13}[c,d]	92.8 ± 0.32	$0.600 \pm 0.011 \times (\theta_{NO_2-S3})$
O_2 adsorption	$k_{II,f}$	5.61[a,b]	0.0	
O_2 desorption	$k_{II,b}$	$9.95 \times 10^{11} \pm 1.75 \times 10^{12}$[c]	44.1 ± 2.6	
NO oxidation	$k_{III,f}$	$1.81 \times 10^{2} \pm 1.54 \times 10^{2}$[a]	12.9 ± 1.4	
NO_2 dissociation	$k_{III,b}$	2.38×10^{12}[c,e]	142.0[e]	$0.784 \times (\theta_{NO_2-S3})$[e]

[a] $m^3/(s\ kg\ zeolite)$.
[b] Calculated from entropy loss.
[c] mol/(s kg zeolite).
[d] Fixed to $10^{13}\ s^{-1}$.
[e] Thermodynamic restriction.

150 °C TPD. Thus, when adsorbing NO_2 at 150 °C there are likely only small amounts of NO_2 species on the copper and instead the more stabile nitrates are formed. During the end of the NO_2 storage (15 min) there is a small NO peak observed experimentally. This is likely due to formation of small amounts of nitrates in the end of the storage phase. The model predicts the nitrate formation and NO release at a higher temperature (115 min). At about 410 °C (138 min) there is a second NO peak, which also the model describes. This is likely due to dissociation of released NO_2 from the nitrates.

In the low-temperature model the oxygen desorption from S3 has a low activation energy, and when the temperature is increased to 50 °C from room temperature the coverage of oxygen on S3 is decreased, which results in a lower production of NO_2. When increasing the temperature even further, the NO oxidation on S3 decreases further and reaches zero at higher temperatures. The mechanism and rates are described in Table 5. The resulting NO, NO_2 and NO_x concentrations when modeling the NO oxidation experiment using both the NO oxidation mechanism and low-temperature mechanism (Eq. (1) and Tables 3–5) are shown in Fig. 8a. The calculated mean coverages on the surface are shown in the lower panel. The model can now describe the NO oxidation over the entire temperature range from room temperature to 500 °C. The model can also describe the NO_x that are released when increasing the temperature. The model predicts NO_2 species on the copper sites, Brönsted acid sites and physisorbed sites already at room temperature. Above 100 °C the coverage of NO_2 on S3 is very low and above this temperature the low-temperature mechanism is not important. The combined model also describes the NO_2 outlet values well between 100 and 250 °C, which the original model did not. The reason is that although the original model had a NO oxidation activity at these temperatures no NO_2 was released due to storage on the surface, which is shown in Fig. 5b. When using the combined model the surface is saturated with NO_x already at room temperature (Fig. 8b) and thus the formed NO_2 between 100 and 250 from the standard NO oxidation model is released.

The kinetic parameters and their linearized 95% confidence intervals are shown in Tables 7 and 8. The NO_2 TPD experiment and NO oxidation experiment were both used to fit the parameters, including the low-temperature NO oxidation.

5. Conclusions

In this study we investigate NO_x adsorption/desorption and NO oxidation over Cu-ZSM-5 using detailed kinetic modeling in combination with flow reactor experiments. NO oxidation is likely an important step both for ammonia SCR and HC-SCR, and so this step is investigated separately. Since the Cu-ZSM-5 catalyst contains both copper and Brönstedt acid sites, the NO_2 adsorption over H-ZSM-5 was also investigated. A simple kinetic model developed based on only one reversible adsorption/desorption reaction step adequately described the NO_2 TPD experiment on H-ZSM-5.

Two TPD experiments, one with NO_2 and the other with NO, were conducted to investigate the NO_x adsorption on Cu-ZSM-5. The catalyst adsorbs large amounts of NO_2. However, the adsorption of NO was substantially lower and therefore the NO adsorption was not included in the model. The NO_2 TPD experiment was used together with one NO oxidation experiment in developing the detailed kinetic model for NO oxidation. Seven reversible reaction steps were used in the model: NO_2 adsorption

on Brönstedt acid sites, NO_2 and O_2 adsorption on copper sites, O_2 dissociation, NO oxidation and two steps for nitrate formation. We found that it was crucial to include two steps for the nitrate formation/dissociation, where the first step was the disproportionation reaction of NO_2 to produce nitrates and NO. In the reverse reaction NO from the gas phase reacts with the nitrates to form NO_2 on the surface. This reaction step lowered the coverage of nitrates in the NO oxidation step, in this case since NO was present in the gas phase; otherwise the high coverage of nitrates would have blocked the surface, resulting in to low NO oxidation. However, we observe that nitrates can be decomposed also without the presence of NO and in the second reversible step was NO_3 decomposed directly to NO_2 and oxygen on the copper sites. Thus using these two steps enabled us to correctly describe both the NO_2 TPD and NO oxidation simultaneously. However, the original model could not describe the NO oxidation below 250 °C and was investigated further.

We observed a low-temperature NO oxidation activity over the Cu-ZSM-5-a catalyst. Even at room temperature significant amounts of NO_2 were produced. However, as the temperature was increased the concentration of NO_2 decreased. At 150 °C the NO oxidation activity began to increase again. We propose that this oxidation occurs with loosely bound species and we have developed a detailed kinetic model that can describe this feature. In addition, one NO_2 TPD at 30 °C was used to develop the storage of NO_2 at low temperature. When using the primary NO oxidation model together with the low-temperature model, we can describe the NO oxidation over the entire temperature range considered, from room temperature to 500 °C.

Acknowledgements

The work is performed at Competence Centre for Catalysis (KCK), Chalmers and at General Motors Research and Development Center. The authors would like to acknowledge helpful discussions with Se Oh, Ed Bissett, Jong-Hwan Lee, Byong Cho and Steven J. Schmieg of the General Motors Research and Development Center and Ashok Gopinath at GM ISL. We would also like to thank GM R&D Center for the financial support. One author (Louise Olsson) would also like to acknowledge the Swedish Research Council (Contract: 621-2003-4149 and 621-2006-3706) for additional support. The financial support from Knut and Alice Wallenberg Foundation for the reactor equipment, Dnr KAW 2005.0055, is gratefully acknowledged.

References

[1] N.-Y. Topsoe, H. Topsoe, J.A. Dumesic, J. Catal. 151 (1995) 226.
[2] J.A. Dumesic, N.-Y. Topsoe, H. Topsoe, Y. Chen, T. Slabiak, J. Catal. 163 (1996) 409.
[3] I.E. Wachs, G. Deo, B.M. Weckhuysen, A. Andreini, M.A. Vuurman, M. de Boer, M.D. Amiridis, J. Catal. 161 (1996) 211.
[4] B. Roduit, A. Wokaun, A. Baiker, Ind. Eng. Chem. Res. 37 (1998) 4577.
[5] E. Tronconi, I. Nova, C. Ciardelli, D. Chatterjee, B. Bandl-Konrad, T. Burkhardt, Catal. Today 105 (2005) 529.
[6] C. Ciardelli, I. Nova, E. Tronconi, D. Chatterjee, B. Bandl-Konrad, M. Weibel, B. Krutzsch, Appl. Catal. B: Environ. 70 (2007) 80.
[7] E. Tronconi, I. Nova, C. Ciardelli, D. Chatterjee, M. Weibel, J. Catal. 245 (2007) 1.
[8] H. Sjövall, L. Olsson, E. Fridell, R.J. Blint, Appl. Catal. B: Environ. 64 (2006) 180.
[9] H. Sjövall, E. Fridell, R.J. Blint, L. Olsson, Topics Catal. 42–43 (1–4) (2007) 113.
[10] L. Olsson, H. Sjövall, R.J. Blint, Appl. Catal. B: Environ. 81 (2008) 203.
[11] H. Sjövall, R.J. Blint, L. Olsson, Accepted for publication, J. of Phys. Chem. C (2008).
[12] J.H. Park, H.J. Park, J.H. Baik, I.-S. Nam, C.-H. Shin, J.H. Lee, B.K. Cho, S.H. Oh, J. Catal. 240 (2006) 47.
[13] K. Rahkamaa-Tolonen, T. Manula, M. Lomma, M. Huuhtanen, R.L. Keiski, Catal. Today 100 (2005) 217.
[14] J.H. Baik, S.D. Yim, I.-S. Nam, Y.S. Mok, J.H. Lee, B.K. Cho, S.H. Oh, Ind. Eng. Chem. Res. 45 (2006) 5258.
[15] G. Delahay, S. Kieger, N. Tanchoux, P. Trens, B. Coq, Appl. Catal. B: Environ. 52 (2004) 251.
[16] S. Kieger, G. Delahay, B. Coq, B. Neveu, J. Catal. 183 (1999) 267.
[17] S. Stevenson, J.C. Vartuli, C.F. Brooks, J. Catal. 190 (2000) 228.
[18] J. Eng, H. Bartholomew, J. Catal. 171 (1997) 27.
[19] M. Devadas, O. Kröcher, M. Elsener, A. Wokaun, N. Söger, M. Pfeifer, Y. Demel, L. Mussman, Appl. Catal. B: Environ. 67 (2006) 187.
[20] O. Kröcher, M. Devadas, M. Elsener, A. Wokaun, N. Söger, M. Pfeifer, Y. Demel, L. Mussman, Appl. Catal. B: Environ. 66 (2006) 208.
[21] B. Coq, M. Mauvezin, G. Delahay, J.B. Butet, S. Kieger, Appl. Catal. B: Environ. 27 (2000) 193.
[22] M. Koebel, G. Madia, M. Elsener, Catal. Today 73 (3–4) (2002) 239.
[23] J.R. Kiovsky, P.B. Koradia, C.T. Lim, Ind. Eng. Chem. Prod. Res. Dev. 19 (1980) 218.
[24] M. Wallin, C.J. Karlsson, M. Skoglundh, A. Palmqvist, J. Catal. 218 (2003) 354.
[25] M. Devadas, O. Kröcher, M. Elsener, A. Wokaun, G. Mitrikas, N. Söger, M. Pfeifer, Y. Demel, L. Mussmann, Catal. Today 119 (2007) 137.
[26] A. Fritz, V. Pitchon, Appl. Catal. B 13 (1997) 1.
[27] R. Burch, J.P. Breen, C.J. Hill, B. Krutzsch, B. Konrad, E. Jobson, L. Cider, K. Eranen, F. Klingstedt, L.E. Lindfors, Topics Catal. 30–31 (1–4) (2004) 19.
[28] Y. Traa, B. Burger, J. Weitkamp, Micropor. Mesopor. Mater. 30 (1999) 3.
[29] M. Shelef, C.N. Montreuil, H.W. Jen, Catal. Lett. 26 (1994) 277.
[30] J.O. Petunchi, W.K. Hall, Appl. Catal. B 2 (1993) L17.
[31] H. Hamada, Y. Kintaichi, M. Sasaki, T. Ito, Appl. Catal. 70 (1991) L15.
[32] I. Halasz, A. Brenner, K.Y. Simon Ng, Catal. Lett. 34 (1995) 151.
[33] X. Wang, S. Yu, H. Yang, S. Zhang, Appl. Catal. B: Environ. 71 (2007) 246.
[34] R. Brosius, D. Habermacher, J.A. Martens, L. Vradman, M. Herskowitz, L. Čapek, Z. Sobalík, J. Dědeček, B. Wichterlová, V. Tokarová, O. Gonsiorová, Topics Catal. 30/31 (2004) 333.
[35] L. Čapek, L. Vradman, P. Sazama, M. Herskowitz, B. Wichterlová, R. Zukerman, R. Brosius, J.A. Martens, Appl. Catal. B: Environ. 70 (2007) 53.
[36] V. Tomašić, Z. Gomzi, S. Zrnčević, Appl. Catal. B: Environ. 18 (1998) 233.
[37] D. Chatterjee, T. Burkhardt, M. Weibel, I. Nova, A. Grossale, E. Tronconi, SAE paper 2007-01-1136 (2007).
[38] H.S. Fogler, Elements of Chemical Reaction Engineering, 3rd ed., 2001.
[39] B. Westerberg, C. Kunkel, C.U.I. Odenbrand, Chem. Eng. J. 92 (2003) 27.
[40] T. Komatsu, M. Nunokawa, I.S. Moon, T. Takahara, S. Namba, T. Yashima, J. Catal. 148 (1994) 427.
[41] W.B. Williamson, D.R. Flentge, J.H. Lunsford, J. Catal. 37 (1975) 258.
[42] W.B. Williamson, J.H. Lunsford, J. Phys. Chem. 80 (1976) 2664.
[43] A. Delabie, K. Pierloot, M.H. Groothaert, B.M. Weckhuysen, A. Schoonheydt, Micropor. Mesopor. Mater. 27 (2000) 209.
[44] A. Grossale, I. Nova, E. Tronconi, Catal. Today 136 (2008) 18.
[45] S.B. Sharma, B.L. Meyers, D.T. Chen, J. Miller, J.A. Dumesic, Appl. Catal. A: Gen. 102 (1993) 253.
[46] L. Olsson, H. Persson, E. Fridell, M. Skoglundh, B. Andersson, J. Phys. Chem. B 105 (2001) 6895.
[47] N. Apostolescu, T. Schröder, S. Kureti, Appl. Catal. B 51 (2004) 43.
[48] Y.H. Yeom, J. Henao, M.J. Li, W.M.H. Sachtler, E. Weitz, J. Catal. 231 (2005) 181.
[49] J. Despres, M. Koebel, O. Kröcher, M. Elsener, A. Wokaun, Appl. Catal. B 43 (2003) 389.
[50] J. Despres, M. Koebel, O. Kröcher, M. Elsener, A. Wokaun, Micropor. Mesopor. Mater. 58 (2003) 175.
[51] G. Centi, S. Perathoner, Catal. Today 29 (1996) 117.
[52] K. Hadjiivanov, D. Klissurski, G. Ramis, G. Busca, Appl. Catal. B: Environ. 7 (1996) 251.
[53] B.J. Adelman, T. Beutel, G.-D. Lei, W.M.H. Sachtler, J. Catal. 158 (1996) 327.